https://doi.org/10.58195/iaet.v2i1.127

Global Science Publishing

IAET

Innovations in Applied Engineering and Technology

https://ojs.sgsci.org/journals/iaet

Article

Stochastic Excitation-Incorporated Seismic Fragility Assessment Using Monte Carlo Simulations

Yi Luo

University of Leeds, Leeds LS2 9JT, UK

Abstract: Structures are susceptible to damage from natural disasters like tornadoes, floods, and seismic events. A resilient structure can withstand such damage and ensure cost-effectiveness. Therefore, accurately assessing the probability of structural failure is imperative for structural designers. This study employs an innovative fragility methodology to assess seismic damage in structures. In comparison to conventional fragility approaches, this method is cost-effective, universally applicable across various seismic sources, and highly precise. Specifically, this method involves the generation of artificial seismic records using the point-source stochastic seismological model and Monte Carlo simulation method. These synthetic seismic records offer distinct advantages when compared to the seismic data collected from real earthquakes at recording stations, such as the ability to adjust the epicentral distance of the synthetic waves as needed. Therefore, this approach enables a comprehensive analysis of structural responses under seismic waves characterized by different attributes. For example, the influence of different seismological parameters such as wave magnitude and epicentral distance are well studied and compared. The advanced finite element software, OpenSees, serves as the computational platform for examining how structures react to diverse seismic waves. The research findings suggest that, compared to traditional methods, utilizing OpenSees can significantly enhance computational efficiency. Furthermore, the methods employed introduce a novel technique for factoring in wave magnitudes and distances during the calculation of structural seismological responses/fragility. This innovation holds significance for the development of next-generation structural resilience designs.

Keywords: resilient structure; fragility; Monte Carlo simulation; seismic

1. Introduction

Structural constructs, including bridges, buildings, and tunnels, frequently endure stochastic forces. Seismic activities and wind loads, which show random fluctuations in both intensity and direction, are particularly significant [1]. To accurately represent these unpredictable forces, it's crucial to convert these loads within the stochastic framework [2]. As highlighted by Yuan, major earthquakes often result in severe casualties and financial losses due to inferior structural performance. Often, the root causes are neglecting seismic effects during design or insufficient fragility evaluations. Structural fragility analysis quantifies the probability of a structure reaching a certain damage level under specific seismic conditions, providing vital insights into potential losses [3]. In this context, Performance-Based Earthquake Engineering (PBEE) is essential, offering a comprehensive fragility assessment of structures while accounting for uncertainties [4]. However, as

Received: 11 November 2023; Accepted: 8 December 2023.

* Corresponding: Yi Luo (13360476789@163.com)

emphasized by Mitseas and Beer, it's crucial to prioritize a structure's ductility rather than merely treating it elastically [2]. Structures face significant forces during earthquakes, often exceeding material elasticity and entering the plastic realm. Evaluations based purely on elasticity might be overly optimistic. In contrast, a structure's ductility can help absorb seismic forces, making nonlinear analyses a more realistic approach.

According to Shinozuka and Deodatis, the Monte Carlo simulation is an effective tool for addressing stochastic challenges [5]. One of its notable strengths is the ability to produce accurate results for problems with deterministic solutions. Nonetheless, a significant drawback is its high computational demand, especially when dealing with nonlinear and varied stochastic problems. To counter these computational demands, many researchers, including Shinozuka, Jeong and Elnashai, and Mitseas and Beer have embarked on relevant studies [2,6,7]. In their extensive random simulations, they've employed strategies to reduce computational loads. These strategies range from optimizing structures, omitting low-impact variables, to using approximate analytical methods.

Additionally, it's worth mentioning that enhancing computational efficiency isn't limited to refining analytical methods. With the recent surge in computer software developments and increased computational power, tools like OpenSees, equipped with High-Performance Computing (HPC) capabilities, can further elevate computational efficiency [8,9].

While numerous researchers have studied the fragility of structures to earthquakes using OpenSees, most have utilized the traditional Incremental Dynamic Analysis (IDA) method, introduced by Vamvatsikos and Fragiadakis [10–13]. This method scales earthquake records' amplitudes to gather extensive earthquake data, predominantly focusing on earthquake acceleration magnitudes. This approach tends to overlook the spatial non-stationarity of seismic actions.

In an effort to more precisely gauge the effects of seismic waves on buildings, Mitseas and Beer employed a vector, comprising magnitude and epicentral distance, as the Intensity Measure (IM) [2]. Drawing from the stochastic point-source earthquake model by Boore, they addressed both temporal non-stationarity and spatial heterogeneity concerns [14]. However, to avoid the extensive computational requirements of Monte Carlo simulations, an approximate nonlinear random dynamic analysis method was chosen. At the heart of this approach lies the averaging out of random processes, simplifying the examination of such systems. Yet, this can result in not comprehensively capturing the seismic wave characteristics, possibly introducing slight discrepancies in the outcomes. Given these conditions, the utilization of artificially synthesized seismic waves becomes more favorable. By gathering a significant amount of seismic wave data and then integrating it into finite element models through efficient tools such as OpenSees, the efficacy of structural assessments can be elevated.

The aim of this study is to develop a novel and precise procedure for the fragility analysis of structures under seismic actions, considering the strengths and weaknesses of existing methodologies. The objectives include conducting a comprehensive review of current structural fragility analysis methodologies, investigating the applicability and merits of the point source stochastic seismological model, examining the unique attributes of earthquakes under various magnitudes and epicentral distances, deriving artificial earthquake records through Monte Carlo simulations, synthesizing earthquake records to enhance understanding of seismic wave properties, achieving familiarity with the OpenSees modelling workflow, applying the newly developed fragility analysis procedure to a multi-degree-of-freedom steel frame, and enriching the understanding of earthquakes and seismic waves based on research findings. Additionally, guidance for future studies in this field will be provided.

2. Methodology

Considering the limitations of existing methods, conducting nonlinear analyses on finite element models using a multitude of artificially-synthesized seismic waves is deemed a more preferable choice. This study introduces a non-elastic, two-dimensional, multi-degree-of-freedom, three-story bending-resistant steel frame structure.

2.1. Stochastic Seismological Model

In the conducted research, the foundation for the Source-based stochastic earthquake model was based on the method Boore had proposed for determining the radiation spectrum and time envelope function of a specific earthquake. The initial step involved determining the earthquake's radiation spectrum [14].

As was outlined in the literature review section concerning the radiation spectrum of the point source earthquake model, the radiation spectrum of the earthquake was determined by four factors: the earthquake source, the propagation path of the earthquake, the distance of the observation site from the earthquake source, and the type of instrument or motion used. The expression for the earthquake radiation spectrum was presented in Equation 1 [14].

$$Y(\omega; M_m; r) = I(\omega)E(\omega, M_0)G(\omega)P(\omega, r) \quad (1)$$

In Equation 1, the variable r represented the horizontal distance between the observation point of the earthquake and its source. Notably, this distance was purely horizontal. M_0 corresponded to the earthquake's moment. The relationship between these two parameters was depicted in Equation 2 [2].

$$M_0 = 10^{1.5(M_m + 10.7)} \quad (2)$$

The description of the earthquake source was as stated in Equation 3 [14].

$$E(\omega, M_0) = CM_0 S_a(M_0, \omega) \times S_b(M_0, \omega) \quad (3)$$

In Equation 3, $S_a(M_0, \omega) \times S_b(M_0, \omega)$ represented the displacement source spectrum of the earthquake, which was a frequency representation of the total energy output of the earthquake. This study adopted the expression used by Atkinson and Silva, as shown in Equation 4 [15].

$$S_a(M_0, \omega) \times S_b(M_0, \omega) = \frac{1-\varepsilon}{1+(\omega/\omega_a)^2} + \frac{\varepsilon}{1+(\omega/\omega_b)^2} \quad (4)$$

In the Equation 4, the ε referred to a weighting parameter. According to the definition of model AS00 in Boore [14], this was a parameter related to the moment magnitude M_m, as shown in Equation 5 [15].

$$\log_{10}\varepsilon = 0.605 - 0.255M_m \quad (5)$$

Furthermore, in Equation 4, ω_a and ω_b represented the lower and upper corner angular frequencies, respectively. When the frequency of the seismic wave was outside the range between these two frequencies, the energy of the seismic wave began to decrease. According to Atkinson and Silva [15], when the moment magnitude M_m was greater than or equal to 2.4, the relationship between ω_a, ω_b, and M_m was as shown in Equations 6 and 7 [15].

$$\log_{10}\omega_a = 2.181 - 0.496M_m \quad (6)$$

$$\log_{10}\omega_b = 2.41 - 0.408M_m \quad (7)$$

Up to this point, the earthquake source was largely defined. The only term that had not been defined in Equation 3 was C, which was identified as a constant in Equation 8 [2].

$$C = \frac{R_\phi VF}{4\pi R_0 \rho_S \beta_S^3} \quad (8)$$

Equation 8 describes the radiation pattern R_ϕ for seismic energy distribution, often expressed as a function of azimuth and take-off angles [16]. For this study, a conservative estimate of 0.55 was recommended for R_ϕ [15]. The term V separates total shear wave energy into horizontal components, with a chosen value of $1/\sqrt{2}$ following Boore's recommendation. The term F accounts for free surface effects, with a recommended value of 2 [14]. Material density ρ_S and shear wave velocity β_S near the seismic source were set at 2.8 g/cm^3 and 3.5 km/s, respectively [15]. The reference distance R_0 in Equation 10 was assigned a value of 1 km based on Boore [14]. To maintain unit consistency, the constant C had to be multiplied by a specific factor (10^{-20}), as advised by Boore [14].

With the seismic source defined, focus shifted to the propagation path of seismic waves. Boore proposed combining the source emission with theoretical path effect calculations, simplifying the path effect as represented in Equation 9 [14].

$$P(\omega, r) = Z(R)\exp(-\pi\omega R/Q(\omega)\beta_s) \quad (9)$$

In Equation 10, it was essential to recognize that R was not identical to the previously mentioned horizontal

distance r. The relationship between R and r was described by Equation 12 [14].

$$R = \sqrt{h^2 + r^2} \tag{10}$$

In Equation 10, h serves as a pseudo-depth for adjusting R, dependent on moment magnitude. The relationship is expressed by Equation 11 [2].

$$\log_{10} h = 0.15M_m - 0.05 \tag{11}$$

In Equation 9, the geometrical spreading function, describing seismic wave energy dissipation over distance, is denoted byω. This function is approximated by piecewise linear segments, expressed in Equation 12 [14]. According to Mitseas and Beer, when R is less than a certain value, R_0 equals 1 [2].

$$Z(R) = \begin{cases} \dfrac{R_0}{R}, & R < R_1 \\ Z(R_1)(\dfrac{R_1}{R})^{p_1}, & R_1 \le R \le R_2 \\ \vdots & \\ Z(R_n)(\dfrac{R_n}{R})^{p_n}, & R \le R_n \end{cases} \tag{12}$$

The remaining component in Equation 9, Q(ω), represents the attenuation factor for seismic wave energy loss during propagation. Its expression is given in Equation 13 [2].

$$Q(\omega) = 680\omega^{0.38} \tag{13}$$

Boore emphasizes the importance of considering local site conditions in seismic wave propagation models, noting their independence from propagation distance in many cases. Equation 14 details the influence of site effects on seismic wave propagation [2,14].

$$G(\omega) = A(\omega)D(\omega) = A_m \exp(-\pi k_0 \omega) \tag{14}$$

Equation 14 represents an amplification coefficient A_m, determined by the relationship between seismic shear wave velocity and depth [14]. Au and Beck suggested assuming it as a constant from empirical curves, especially for generic rock conditions, expressed as: $A(\omega) = A_m = 2.5$ [17].

The coefficient D(ω) represents attenuation, capturing energy loss in high-frequency seismic motions. Boore emphasized the path-independence of this loss, indicating consistency regardless of geological variations or propagation distance [14]. Based on the recommendation by Mitseas and Beer, a value of k_0= 0.015 was deemed appropriate [2].

Lastly, the definition of the type of ground motion had not been completed. As was suggested by Boore, a filter was recommended to simulate the specific characteristics of the ground motion. The principle behind the filter was illustrated in Equation 15 [14].

$$I(\omega) = (2\pi\omega i)^n \tag{15}$$

According to Boore, n could assume the values 0, 1, or 2, corresponding to ground displacement, velocity, and acceleration, respectively [14].

Boore suggests two methods for obtaining ground motion from the radiation spectrum: "time-domain simulation" and stochastic vibration theory [14]. The first method simulates earthquakes in detail, while the second estimates peak motion more efficiently. Mitseas and Beer found the acceleration time series' envelope function (Equation 16) effective in earthquake simulations [2].

$$e(t; M_m; r) = \alpha(t/t_n)^b \exp(-c(t/t_n)) \tag{16}$$

In Equation 16, α, b, and c were parameters, defined respectively by Equations 17, 18, and 19 [2].

$$\alpha = [\exp(1)/\lambda]^b \tag{17}$$

$$b = -\lambda \ln(\eta)/[1 + \lambda(\ln(\lambda) - 1)] \tag{18}$$

$$c = b/\lambda \tag{19}$$

From Equations 17 to 19, λ and η were selected based on the recommendation by Mitseas and Beer as $\lambda = 0.2$ and $\eta = 0.05$, respectively [2]. Furthermore, in Equation 16, t_n was related to ω_a, representing the lower corner angular frequency of the seismic wave. This relationship was detailed in Equation 20 [2].

$$t_n = 0.1R + 2\pi/\omega_a \tag{20}$$

2.2. Evolutionary Power Spectrum

Based on the research by Mitseas and Beer, once the radiation spectrum and time envelope function of the ground motion were established, the evolutionary power spectral density function describing the earthquake could be derived from Equation 21 [2]. This function was intimately related to the seismic moment and epicentral distance, and was characterized by two independent variables: angular frequency and time.

$$S_{\ddot{\alpha}_g}(\omega, t) = \left| e(t; M_m; r) \right|^2 Y(\omega; M_m; r) \tag{21}$$

2.3. Generation of Compatible Artificial Earthquake Records

Based on the defined power spectral density function for earthquake-induced motion, the method by Shinozuka and Deodatis was employed to produce sample functions of this stochastic process [5]. Essentially, their technique centered on swiftly producing sample functions of the stochastic process using a cosine series formula, as shown in Equation 22 [5].

$$f(t) = \sqrt{2} \sum_{n=0}^{N-1} A_n \cos(\omega_n t + \phi_n) \tag{22}$$

In Equation 22, ϕ_n was represented as the random phase angle, and its value ranged from 0 to 2π. It was emphasized that ϕ_n was an independent random number [5]. Besides, $A_n$was closely related to the power spectral density function of the ground motion. Their relationship was illustrated in Equation 23 [5].

$$A_n = \sqrt{(2S_{f_0 f_0}(\omega_n)\Delta\omega)}, \qquad n = 0, 1, 2, 3, \cdots, N-1 \tag{23}$$

In Equation (25), ω_n was identified as a subset of the independent variable ω from the evolutionary power spectral density function of the ground motion. As defined by Shinozuka and Deodatis, if the angular frequency exceeded this value, the evolutionary power spectral density function was considered to be zero [5]. The detailed relationships were depicted in Equations 24 and 25 [5].

$$\omega_n = n\Delta\omega, \qquad n = 0, 1, 2, 3, \cdots, N-1 \tag{24}$$

$$\Delta\omega = \frac{\omega_u}{N}, \qquad n = 0, 1, 2, 3, \cdots, N-1 \tag{25}$$

In Equation 25, ω_u was ascertained by Equation 26. As recommended by Shinozuka and Deodatis [5], ε was set to 0.001. Equation 26 was detailed below.

$$\int_0^{\omega_u} S_{f_0 f_0}(\omega) d\omega = (1-\varepsilon) \int_0^{\infty} S_{f_0 f_0}(\omega) d\omega \tag{26}$$

2.4. Modeling Using OpenSees

Using OpenSees, a single-span, three-story high 2D steel moment-resisting frame was constructed. Relying on Saruddin and Nazri's recommendations, the frame possessed a height of 3m per story and a 5m span [10]. S275 steel was utilized. The steel beam and column dimensions were 533×210×109 and 305×305×198, respectively, with detailed specifications sourced from the British Constructional Steelwork Association and Steel [18]. The Schematic Representation and Cross-sectional View of the Steel Frame are presented in Figure 1.

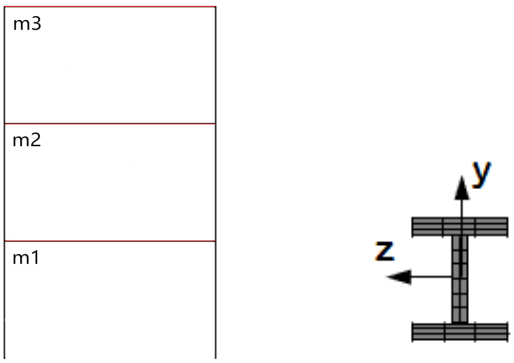

Figure 1. Schematic Representation and Cross-sectional View of the Steel Frame.

In the parameter-setting step, units (m, N, sec) were defined for computations. Loops were established to comprehensively consider magnitude and epicentral distance combinations in a point-source earthquake model, utilizing the `foreach` command for efficient iteration.

In the second step, fundamental settings configured the model as 2D (`ndm 2`) with three degrees of freedom per node (`ndf 3`). Various scripts, including visualization commands, were imported.

The third step defined nodes and mass. A frame structure was characterized with specific properties, nodes were created, and boundary conditions were set. Nodal mass was distributed evenly using the `mass` command.

The fourth step focused on material properties. Steel 02 was chosen for its ability to simulate cyclic steel behavior, considering the Bauschinger effect. Parameters like yield strength (Fy), elastic modulus (E0), and others were specified based on OpenSees Wiki recommendations. The details were presented in Figure 2 [19].

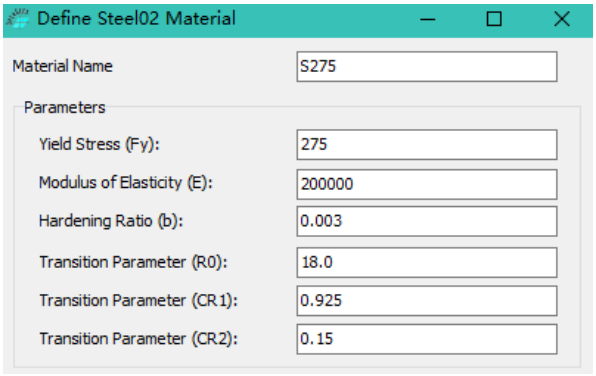

Figure 2. Details of Steel 02.

In the fifth step, section properties were defined using dimensional information from reputable sources. Calculations determined auxiliary parameters, such as the web depth for columns and beams. The `section fiberSec` command was then used to create fiber sections, segmented into web and flanges using the `patch quadr` command. Material from the fourth step was assigned to these sections, and the `element nonlinearBeamColumn` command defined nonlinear beam-column elements.

The sixth step involved gravity and eigenvalue analyses. A gravity loading pattern was defined, and a static analysis ensured structural stability. The Newton-Raphson method facilitated convergence. Eigenvalue analysis determined natural frequencies and vibration periods, essential for understanding dynamic responses.

In the seventh step, structure damping was defined using the Rayleigh command, assuming proportionality to both mass and stiffness (Equation 27, 28 and 29) [20].

$$C = \alpha M + \beta K \tag{27}$$

$$\alpha = \xi \frac{2\omega_1 \omega_2}{\omega_1 + \omega_2} \tag{28}$$

$$\beta = \xi \frac{2}{\omega_1 + \omega_2} \tag{29}$$

In Equations 28 and 29, ξ represents the damping ratio, typically set at 0.05. The structure's stiffness wasn't directly specified; as the cross-section was a fiber section, OpenSees automatically calculated overall stiffness through fiber integration.

In the eighth step, seismic actions were inputted, and structural responses were outputted. Earthquake waves were obtained from Monte Carlo simulations, with 20 waves per combination of epicentral distance and seismic source. The Drift Recorder command logged inter-story drift ratios for structural performance evaluation. Node displacements were recorded using the Recorder Node command. The Fiber Stress-Strain Recorder command captured stress-strain relationships in fiber sections. The tfinal command displayed the total duration of structural analysis.

2.5. Post-processing of Data and Structural Fragility Analysis

After completing the eight mentioned stages, the nonlinear time-history analysis yielded results, including

inter-story drift ratios, critical node displacements, fiber section stress-strain relationships, and the total analysis duration. The Structural Engineers Association of California categorizes the performance levels of steel structures into five levels based on inter-story drift ratios, as outlined in Table 1 [21].

Table 1. Performance Levels Based on Drift Ratios (Ghobarah).

Performance level	Damage state	Drift
Fully operational, Immediate occupancy	No damage	<0.2%
Operational, Damage control, Moderate	Repairable	<0.5%
Life safe - Damage state	Irreparable	<1.5%
Near collapse, Limited safety, Hazard reduced	Severe	<2.5%
Collapse		>2.5%

According to Mitseas and Beer, when the Intensity Measure (IM) in the structural fragility analysis was defined as a vector possessing both epicentral distance and magnitude characteristics [2], the three-dimensional fragility surface of the structure could be obtained through Equation 30.

$$P_{ls}[\delta(t) \geq \delta_{ls} = \delta \,|\, IM(M_m, r)] = 1 - \int_0^{\delta} p(\delta(t) \,|\, IM(M_m, r)) d\theta \quad (30)$$

2.6. Brief Summary

This chapter provided a detailed explanation of earthquake radiated spectra, time envelope functions, and evolving power spectral density functions, clarifying the parameters involved. The synthesis of earthquake records was discussed, employing the cosine series formula and Monte Carlo simulations. Material choices and steps for constructing a three-story, two-dimensional steel moment-resisting frame in OpenSees were outlined. The chapter concluded by introducing criteria for evaluating structural fragility and utilizing the inter-story drift ratio to form a three-dimensional fragility surface. The subsequent chapter will present results derived from these methodologies, featuring in-depth analyses to enhance the interpretation of findings.

3. Research Results and Data Analysis

This chapter aligns with the methodology, starting with an introduction to the radiation spectrum and time envelope function of the point source seismic model. It then presents illustrations of the evolving power spectral density function and showcases a subset of earthquake waves simulated using Shinozuka and Deodatis's method [5]. The chapter concludes by presenting the fragility surface of nonlinear structures under seismic actions and conducting a detailed analysis of structural fragility under various standards.

3.1. The Radiation Spectrum and Time Envelope Function of the Stochastic Seismic Model

Yeats et al established a correlation between Richter magnitudes and earthquake effects. Magnitudes of 2 or lower were generally imperceptible, while magnitude 3 caused minor tremors near the epicenter [22]. Magnitude 4 induced noticeable shaking, with rare structural harm. Magnitude 5 led to minor damages like wall cracks, and magnitude 6 posed a threat, potentially causing sections to crumble. At magnitude 7, even seismic buildings faced potential damages, and magnitudes 8 or higher posed risks to virtually all structures. This research examined earthquakes with magnitudes between 5 and 8 due to their damage potential. The selection of epicentral distance for earthquakes follows the model by Mitseas and Beer, considering a range of 10 km to 80 km as reasonable [2].

The radiation spectrum of the earthquake with a constant epicentral distance is depicted in Figure 3.

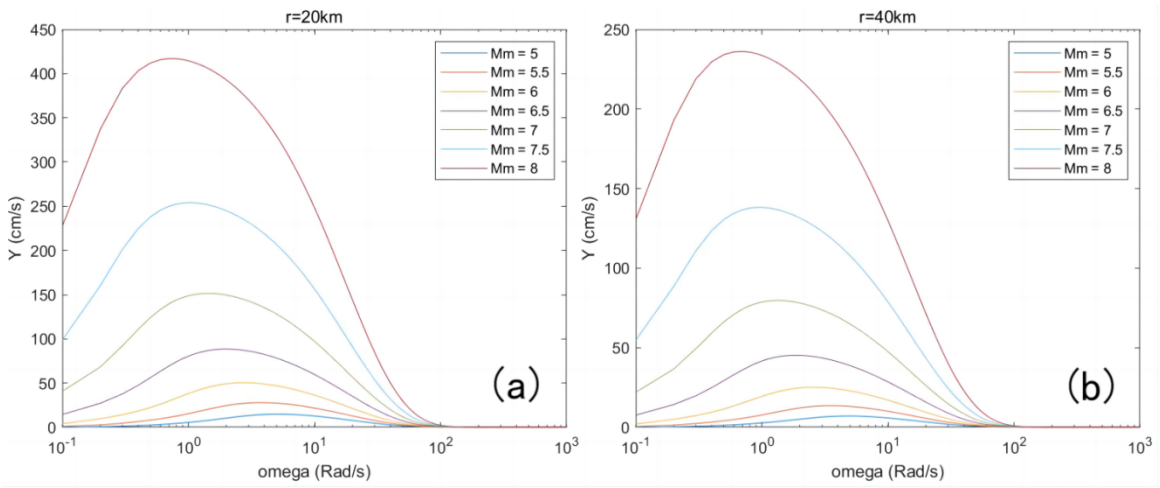

Figure 3. Radiated spectrum for various Mm values at (a) r=20km, (b) r=40km.

Figure 3 shows significant similarities, revealing key insights: 1. The Y-axis represents the radiated spectrum intensity. Across all figures, as earthquake magnitude (Mm) increases (from 5 to 8), the peak Y value rises, indicating larger magnitude earthquakes release more energy. 2. With higher Mm, the frequency (f) corresponding to the peak of Y decreases, suggesting higher magnitude earthquakes tend to have lower-frequency peak radiated spectra. 3. Each figure corresponds to a distinct epicentral distance (20km to 80km). Regardless of magnitude, the peak Y value decreases as epicentral distance expands, indicating diminishing earthquake intensity with distance from the epicenter.

The time envelope functions corresponding to various epicentral distances, with a constant magnitude, are illustrated in Figure 4.

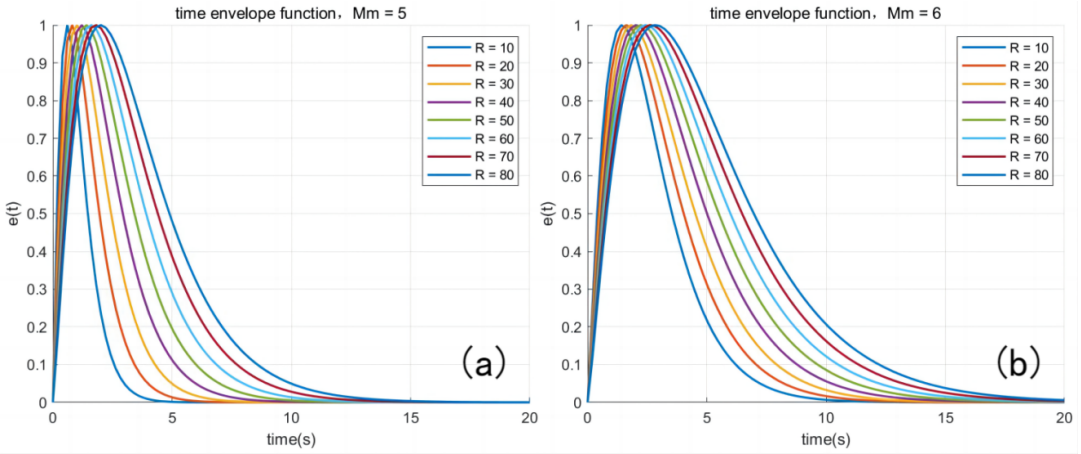

Figure 4. Time envelope function of the earthquake when (a) Mm= 5, (b) Mm= 6.

Analyzing Figure 4.6's maximum points, their corresponding times, and the relationship between e's amplitude, R, and Mm, along with examining the function's duration for each R and Mm value, yields the following observations: 1. Increasing epicentral distance (R) leads to a delay in the time for the function to reach its peak, indicating more distant regions experience intense shaking later. 2. Higher Mm results in an extended time to reach the peak, reflecting the broader fault area and longer rupture durations of high-magnitude earthquakes. This leads to the dispersal of energy over a lengthier time compared to low-magnitude events. 3. Generally, the peak amplitude of e is observed to be near 1.

3.2. The Evolutionary Power Spectrum of the Stochastic Seismic Model

Figure 5 displays the evolving power spectral density functions for specific combinations of magnitude and epicentral distance.

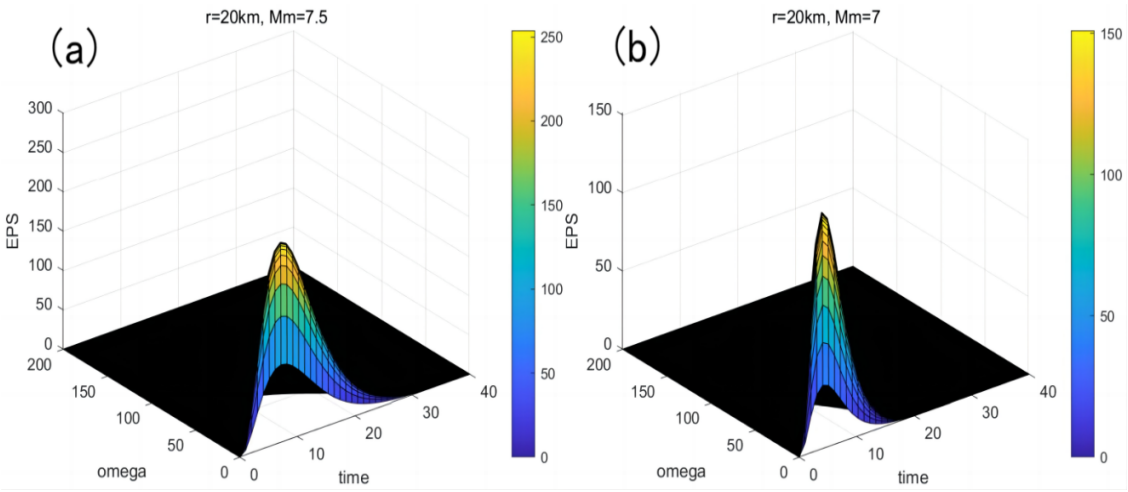

Figure 5. Evolving power spectral density function for specific combinations of epicentral distance and magnitude.

3.3. Artificially Simulated Earthquake Records

Cosine series formula was employed to generate earthquake records [5]. Following Yeats et al and Mitseas and Beer, records were produced for magnitudes between 5 and 8 (increasing by 0.5) and epicentral distances from 10km to 80km (in 10km steps) [2,22]. Each magnitude-distance combination yielded 20 records, totaling 1, 120 earthquake waves. Besides, peak acceleration is an essential parameter for the generated earthquake waves. Figure 6 illustrates the range of peak accelerations recorded from synthetic earthquakes for some particular combinations of epicenter distance and magnitude.

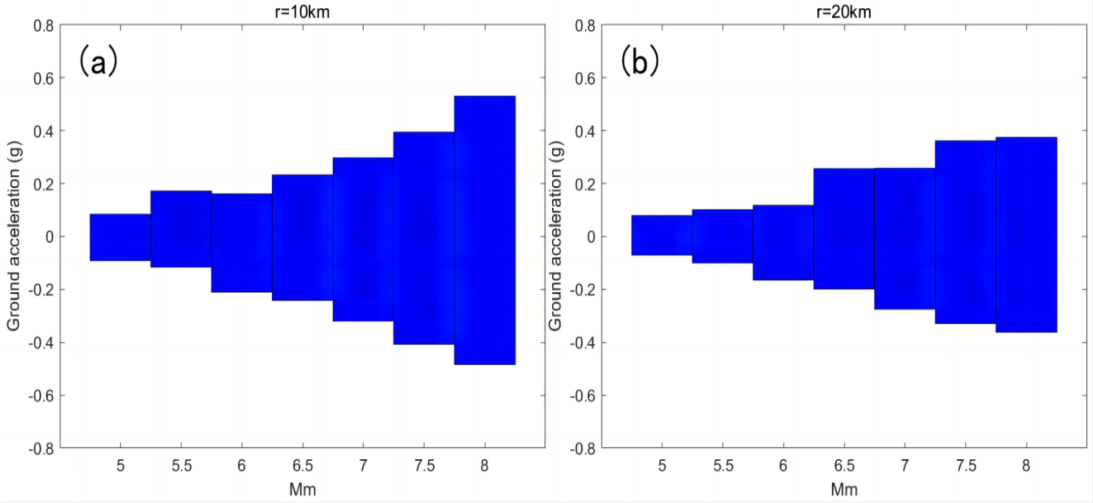

Figure 6. Peak Accelerations Range for Synthetic Earthquake Records.

Figure 6 illustrates the peak acceleration range for synthetically generated earthquake records at various magnitudes while maintaining a constant epicentral distance. Clearly, as the magnitude increases under a constant epicentral distance, there is a noticeable upward trend in acceleration.

3.4. Structural Fragility Analysis

Based on the inter-story drift ratio exported from the recorder command in OpenSees, combined with the standards for assessing structural fragility defined, the three-dimensional fragility surface of the structure was obtained using Matlab, as depicted in Figure 7.

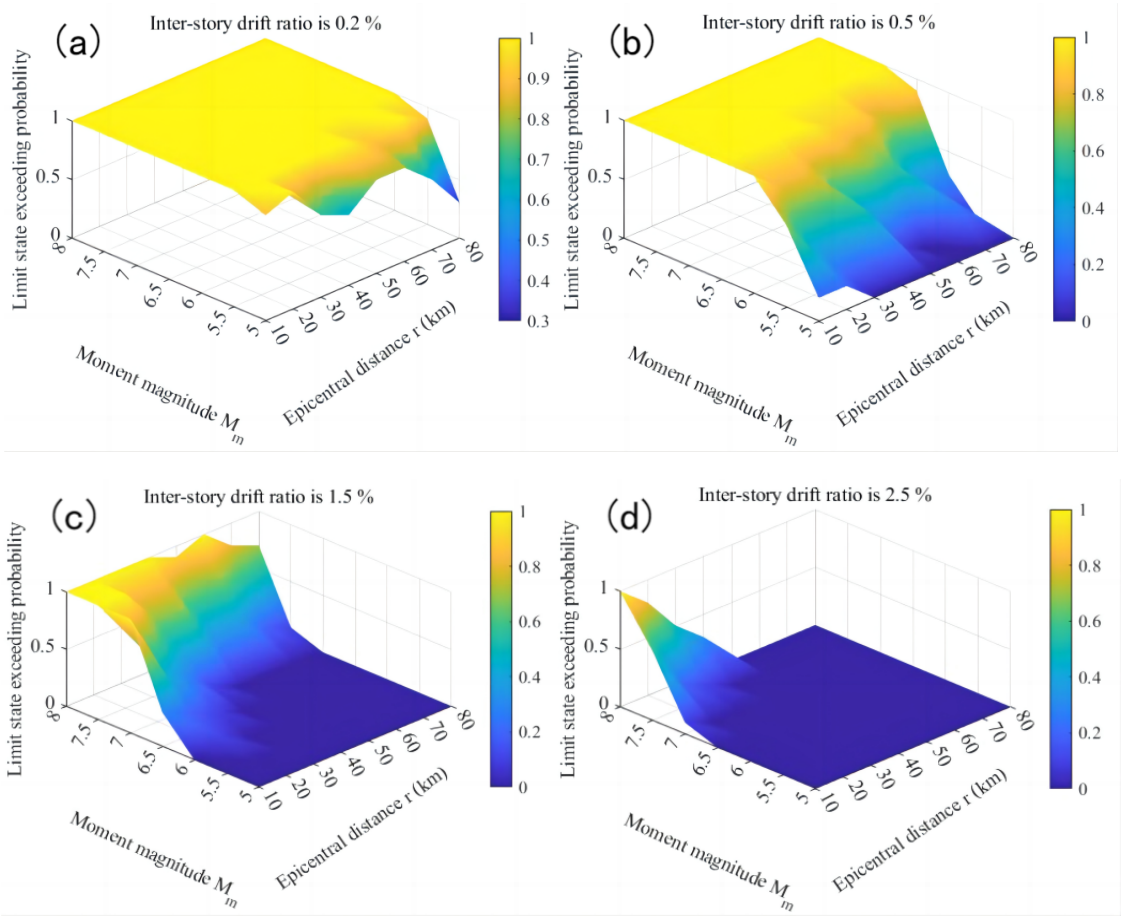

Figure 7. 3D Fragility Surface from Inter-Story Drift Ratios and Assessment Standards.

Figure 7 reveals distinct patterns: (1) Keeping the epicentral distance constant, the probability of the structure's inter-story drift ratio exceeding the threshold increases with higher earthquake magnitudes. (2) Conversely, maintaining a steady magnitude, an increase in the epicentral distance also raises the likelihood of the inter-story drift ratio surpassing the threshold.

It should be noted that according to the OpenSees time recorder, solving the effect of a single earthquake wave on the steel anti-bending frame takes approximately 4 seconds. The laptop specifications include an i7-9750H processor with 6 cores clocked at 2.6GHz, 16GB DDR4 RAM at 3200Hz, and Windows 10 Professional, 64-bit operating system.

Additionally, Figure 8 illustrates the stress-strain relationship for the Steel 02 material defined in this study under the influence of an earthquake wave with an epicentral distance of 10km and a magnitude of 8.

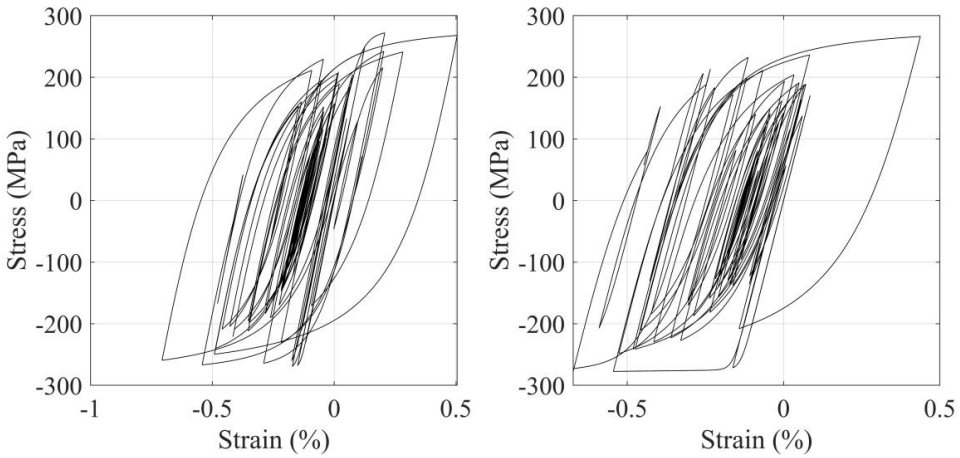

Figure 8. Stress-Strain Behavior of Steel 02 Material

4. Conclusion

This study aimed to enhance the accuracy and efficiency of structural fragility analysis under seismic activities. It used OpenSees, showing improved computational efficiency compared to prior methods. The Monte Carlo simulation precision was reliable. The study provided detailed insights into methodologies, revealing characteristics of earthquakes and seismic waves.

The secondary objectives were largely met, with comprehensive explanations of methodologies, OpenSees modeling, and fragility surface visualization. The analysis yielded conclusions on seismic characteristics, such as energy release, frequency range, and acceleration variations. Some limitations include neglecting near-field waves, large increments in seismic wave fitting, lack of robust validation for fragility surfaces, and unexplored potential for parallel processing in computational efficiency enhancement.

Future research could address these limitations, considering near-field waves, refining seismic wave fitting increments, validating fragility surfaces comprehensively, and exploring parallel processing benefits in computational efficiency.

Funding

Not applicable.

Institutional Review Board Statement

Not applicable.

Informed Consent Statement

Not applicable.

Data Availability Statement

Not applicable.

Acknowledgments

I would like to extend my deepest gratitude to Doctor Ioannis P. Mitseas. Without his relentless guidance and vast expertise, this challenge would have been immensely difficult for me to overcome, especially in the area of artificially synthesizing earthquake records. He timely corrected a directional mistake I had made, for which I am immensely grateful.

Conflicts of Interest

The author declares no conflict of interest.

Reference

1 Spanos PD, Vargas Loli LM. A Statistical Approach to Generation of Design Spectrum Compatible Earthquake Time Histories. *International Journal of Soil Dynamics and Earthquake Engineering* 1985; **4** (**1**): 2–8.

2 Mitseas IP, Beer M. Fragility Analysis of Nonproportionally Damped Inelastic MDOF Structural Systems Exposed to Stochastic Seismic Excitation. *Computers & Structures* 2020; **226**: 106129.

3 Xin D, Daniell JE, Wenzel F. Review Article: Review of Fragility Analyses for Major Building Types in China With New Implications for Intensity–PGA Relation Development. *Natural Hazards and Earth System Sciences* 2020; **20**(**2**): 643–672.

4 Mitseas IP, Kougioumtzoglou IA, Beer M. An Approximate Stochastic Dynamics Approach for Nonlinear Structural System Performance-Based Multi-Objective Optimum Design. *Structural Safety* 2016; **60**: 67–76.

5 Shinozuka M, Deodatis G. Simulation of Stochastic Processes by Spectral Representation. *Applied Mechanics Reviews* 1991; **44**(**4**) 191–204.

6 Shinozuka M, Feng MQ, Kim H-K, Kim S-H. Nonlinear Static Procedure for Fragility Curve Development. *Journal of Engineering Mechanics* 2000; **126**(**12**): 1287–1295.

7 Jeong S-H, Elnashai AS. Probabilistic Fragility Analysis Parameterized By Fundamental Response Quantities. *Engineering Structures* 2007; **29**(**6**): 1238–1251.

8 Wikipedia. List of Intel Core i7 Processors. Available online: https://en. wikipedia. org/wiki/List_of_Intel_Core_i7_processors (accessed on 20 August 2023).

9 McKenna F. OpenSees: A Framework for Earthquake Engineering Simulation. *Computing in Science & Engineering* 2011; **13**(**4**): 58–66.

10 Saruddin SNA, Nazri FM. Fragility Curves for Low- and Mid-rise Buildings in Malaysia. *Procedia Engineering* 2015; **125**: 73–878.

11 Xu C, Deng J, Peng S, Li C. Seismic Fragility Analysis of Steel Reinforced Concrete Frame Structures Based on Different Engineering Demand Parameters. *Journal of Building Engineering* 2018; **20**: 736–749.

12 Zhao Y, Hu H, Bai L, Tang M, Chen H, Su D. Fragility Analyses of Bridge Structures Using the Logarithmic Piecewise Function-Based Probabilistic Seismic Demand Model. *Sustainability* 2021; **13**(**14**): 7814–7814.

13 Vamvatsikos D, Fragiadakis M. Incremental Dynamic Analysis for Estimating Seismic Performance Sensitivity and Uncertainty. *Earthquake Engineering & Structural Dynamics* 2009; **39**(**2**): 141–163.

14 Boore DM. Simulation of Ground Motion Using the Stochastic Method. *Pure and Applied Geophysics*. 2003; **160**(**3**): 635–676.

15 Atkinson GM, Silva W. Stochastic Modeling of California Ground Motions. *Bulletin of the Seismological Society of America* 2000; **90**(**2**): 255–274.

16 Boore DM, Boatwright J. Average Body-Wave Radiation Coefficients. *Bulletin of the Seismological Society of America*. 1984; **74**(**5**): 1615–1621.

17 Au SK, Beck JL. Subset Simulation and its Application to Seismic Risk Based on Dynamic Analysis. *Journal of Engineering Mechanics-asce* 2003; **129**(**8**); 901–917.

18 British Constructional Steelwork Association and Steel. *Steel building design: design data: in accordance with Eurocodes and the UK National Annexes*; Steel Construction Institute: Ascot, Berkshire, London, 2015.

19 OpenSees Wiki. Steel02 Material -- Giuffré -Menegotto-Pinto Model with Isotropic Strain Hardening - OpenSeesWiki. Berkeley. edu. Available online: https://opensees. berkeley. edu/wiki/index. php/Steel02_Material_--_Giuffr%C3%A9-Menegotto-Pinto_Model_with_Isotropic_Strain_Hardening (accessed on 12 August 2023).

20 Charney FA. Unintended Consequences of Modeling Damping in Structures. *Journal of Structural Engineering* 2008; **134**(**4**): 581–592.

21 Structural Engineers Association of California. Performance-based Seismic Engineering of Buildings. *Vision 2000 Report* 1995.

22 Yeats RS, Sieh KE, Allen CR. *The Geology of Earthquakes*. Oxford University Press: New York, NY, USA, 1997.